Thin Solid Films 701 (2020) 137950

Contents lists available at ScienceDirect

Thin Solid Films

journal homepage: www.elsevier.com/locate/tsf

Improved interface quality of atomic-layer-deposited ZrO_2 metal-insulator-metal capacitors with Ru bottom electrodes

Jae Hwan Lee[a], Bo-Eun Park[a], David Thompson[b], Myeonggi Choe[c], Zonghoon Lee[c], Il-Kwon Oh[a,*], Woo-Hee Kim[d,*], Hyungjun Kim[a,*]

[a] School of Electrical and Electronics Engineering, Yonsei University, Seoul, 03722, Korea
[b] Applied Materials, Sunnyvale, California 94085, USA
[c] School of Materials Science and Engineering, Ulsan National Institute of Science and Technology, Ulsan 44919, Republic of Korea
[d] Department of Materials Science and Chemical Engineering, Hanyang University, 55 Hanyangdeahak-ro, Sangnok-gu, Ansan, Gyeonggi-do 15588, Republic of Korea

ARTICLE INFO

Keywords:
Zirconium oxide
Atomic layer deposition
Metal-Insulator-Metal
Titanium nitride
Ruthenium
Interfacial layer

ABSTRACT

We investigate effects of bottom electrodes on ZrO_2 thin films formed through atomic layer deposition (ALD). We focus on the correlation between interfacial layer formation and electrical properties. For this comparative study, two different bottom electrodes consisting of TiN and Ru were employed. ALD ZrO_2 films are deposited on these bottom electrodes by using tris(dimethylamino)cyclopentadielnyl zirconium ($(C_5H_5)Zr[N(CH_3)_2]_3$) and ozone as a precursor and oxidant, respectively. Based on detailed investigations using transmission electron microscopy and X-ray photoelectron spectroscopy, we are able to comparatively characterize the formations and chemical compositions of the interfacial layers between ALD ZrO_2 and both bottom electrodes. Based on the electrical properties of metal-insulator-metal capacitors fabricated using both the TiN and Ru bottom electrodes, we observe improved capacitance-voltage and current-voltage characteristics with the Ru bottom electrode, which are attributed to the suppressed formation of an interfacial layer. We also discuss the correlation between traps in the interfacial layer and electrical properties.

1. Introduction

Over the past few decades, dynamic random access memory (DRAM) capacitor techniques have been developed through down-scaling and three-dimensional structuring [1]. In particular, structural changes in metal-insulator-metal (MIM) capacitors and the introduction of high-*k* dielectrics in conjunction with TiN electrodes have significantly improved the electrical properties of sub-100-nm processes. Various high-*k* dielectric layers, including HfO_2 [2], $SrTiO_3$ [3], TiTaO [4], $Zr_{(1-x)}Al_xO_2$ [5], Ta_2O_5 [6], La_2O_3 [7], Al_2O_3 [8], and $HfSi_xO_y$ [9] have been combined with TiN electrodes in MIM capacitors and investigated for the purpose of enhancing memory-cell density in DRAM. Among the materials above, ZrO_2 has attracted enormous attention for DRAM capacitor dielectrics by virtue of its high enough dielectric constant (ε_r = ~25), wide band gap (5.1–7.8 eV), and good thermodynamic stability [10,11]. In comparison to HfO_2, moreover, it is advantageous for transformation into cubic or tetragonal phases with higher dielectric constant at relatively lower crystallizing temperature for higher capacitance density [12]. For these reasons, it has been adopted as the main dielectric material in DRAM cells with a design rule of <~70 nm. However, a single ZrO_2 dielectric layer does not satisfy the requirements of a capacitance density greater than 7 fF μm^{-2} and leakage current density less than 10^{-8} A cm^{-2} for MIM capacitors for DRAM, which were defined in 2016 [13]. For sub-60-nm processes, a $ZrO_2/Al_2O_3/ZrO_2$ structure has emerged as the top choice for commercial DRAM products [14].

When a high-*k* dielectric thin film is deposited on a TiN electrode, controlling interfacial layer formation between the dielectric layer and metal electrode is crucial. Generally, interfacial layers have high defect densities that create charge traps, resulting in the degradation of device performance [15]. For example, when high-*k* dielectric films are deposited on TiN using atomic layer deposition (ALD), oxygen-deficient TiO_x layers, which degrade electrical properties, are formed at the interface based on the high chemical reactivity of the bottom TiN layer during oxide deposition [16]. Accordingly, introducing a suitable surface treatment may help to promote the formation of a stable interfacial layer between TiN electrodes and high-*k* dielectrics. For example, post-plasma treatment using N_2 plasma or mixed N_2/O_2 plasma on TaN electrodes has been shown to suppress the formation of unwanted interfacial layers [17]. However, when electrodes are exposed to plasma

* Corresponding authors.
E-mail addresses: ikoh@yonsei.ac.kr (I.-K. Oh), wooheekim@hanyang.ac.kr (W.-H. Kim), hyungjun@yonsei.ac.kr (H. Kim).

https://doi.org/10.1016/j.tsf.2020.137950
Received 1 September 2019; Received in revised form 14 March 2020; Accepted 15 March 2020
Available online 16 March 2020

treatment, they are subject to being damaged by energetic species, such as ions and radicals [18]. Additionally, it is difficult to apply plasma treatment to the mass production of DRAM because non-uniform treatment is anticipated for MIM devices formed inside deep trenches with high aspect ratios.

Alternatively, the adoption of stable metal electrodes with high work functions, such as Pt and Ir, can improve dielectric properties [19,20]. It has been shown that the use of a Ru electrode is a promising option based on its good thermal and chemical stability, low resistivity (ρ_{bulk} = 7.6 μΩ cm), high work function (Φ_{bulk} = 4.71 eV), and relatively cheap cost among noble metals [21,22]. For example, a previous study examined the effects of Ru buffer layer growth on a TiN electrode for TiO_2-based MIM capacitors. The Ru buffer layer resulted in improved electrical properties compared to a simple TiN bottom electrode [23]. In another report, Ru/Ta_2O_5/Ru MIM capacitors were investigated and found to provide good electrical performance [24]. However, the interfaces and electrical properties of ALD ZrO_2 processes in conjunction with Ru bottom electrodes have rarely been studied in comparison to those with TiN electrodes. This motivated us to comparatively investigate the dielectric properties of ALD ZrO_2 on TiN and Ru bottom electrodes.

In this paper, therefore, we report the effects of bottom electrodes on the thin film properties of ALD ZrO_2. We focus on the correlation between interfacial layer formation and electrical properties. Film thickness, microstructures, and chemical compositions are characterized by transmission electron microscopy (TEM) and X-ray photoelectron spectroscopy (XPS). The electrical properties of MIM capacitors fabricated using both the TiN and Ru bottom electrodes are evaluated through capacitance–voltage (*C–V*) and current–voltage (*I–V*) measurements. The correlation between charge traps in the interfacial layer and electrical properties is also discussed.

2. Experimental details

We deposited 100-nm-thick TiN and Ru layers for bottom electrodes by using DC magnetron sputtering with 30 W of plasma power (SNTEK Co., RSP 5003) on SiO_2/Si substrates. We used a commercial showerhead-type ALD chamber (SNTEK Co., ALD5008) for the ALD ZrO_2 thin film process with tris(dimethylamino)cyclopentadielnyl zirconium (ZyALD$^{TM:}$ $(C_5H_5)Zr[N(CH_3)_2]_3$) as a Zr precursor (Air Liquide Co.) and O_3 (11%) as an oxidizing agent. To produce sufficient vapor pressure, the temperature of the Zr precursor was maintained at 70 °C in a stainless-steel bubbler. An Ar carrier gas was used to deliver the Zr precursor vapors into the reaction chamber. Its flow rate was maintained at 50 $cm^3\ min^{-1}$ by a mass flow controller. To evacuate excess molecules and byproducts from the reaction chamber between each precursor and reactant exposure step, the same flow rate of Ar gas was used again. The ALD process sequence for ZrO_2 followed a pattern of 2-5-1-5 s and showed a typical ALD growth mode with saturated growth rates of 0.8 Å $cycle^{-1}$. During the ALD experiments, the substrate temperature was maintained at 180 °C.

The film thicknesses and microstructures were characterized through TEM (FEI, Titan cubed G2 60-300) observation with a 200-kV acceleration voltage. Impurity levels, chemical compositions, and binding structures were analyzed using XPS (K-alpha, Thermo VG, U.K.) with an Al Kα (1486.6 eV) monochromatic source (sampling area diameter of 400 μm). All binding energies were arranged with respect to C 1s (284.5 eV) to calibrate the spectrum energy. For XPS depth profile analysis, the specimens were sputtered using an Ar^+ ion gun (energy of 0.5 keV; induced beam current: 3 mA; rastered over a 2 × 2 mm^2 area). The XPS data was analyzed using the Spectral Data Processor (SDP) (Version 4.11, XPS International LLC, Mountain View, CA). In its structure, the SDP software uses for the deconvolution of the XPS line a specific ratio between the Lorentzian and Gaussian shape, and these characteristics ensures a good fit of experimental data.

To fabricate MIM capacitors, 10-nm-thick ALD ZrO_2 dielectric films were deposited on both the TiN and Ru bottom electrodes, followed by post-deposition annealing for 10 min at 400 °C in a tube furnace with an N_2 atmosphere. Next, a 100-nm-thick Ru top electrode was deposited via DC magnetron sputtering with a plasma power of 30 W. A patterned shadow mask was used to define a contact area with a contact radius of 100 μm. Electrical properties based on *C–V* and *I–V* characteristics were measured using an HP 4284A *C–V* analyzer (frequency ranges from 1 kHz to 1 MHz) and an Agilent semiconductor parameter analyzer (Agilent B1500A, Agilent Technologies), respectively.

Table 1
Properties of (a) TiN and (b) Ru metal electrodes.

Bottom Electrode	Resistivity (μΩ cm)	Work Function (eV)
TiN	11	4.30
Ru	7.6	4.71

3. Results and discussion

We investigate the interface properties of ALD ZrO_2 thin films on TiN and Ru bottom electrodes (Table 1). Fig. 1(a) and (b) present cross-sectional TEM images of ZrO_2 on TiN and Ru, respectively, following 185 cycles of ZrO_2 ALD. The total film thickness of both samples is approximately 15 nm, but there is a notable difference in the thicknesses of the interfacial layers. From Fig. 1(a) and (b), one can see that the thickness of the interfacial layer on TiN is approximately 3 nm, whereas that on Ru is almost negligible because the Ru inhibited the formation of an interfacial layer. Interfacial layers between metal electrodes and oxide materials can be formed from oxidation and oxygen diffusion. Oxidation of the electrode surface by oxygen species induce an interfacial layer formation during film deposition [25]. Interface oxidation depends on the potential barrier height to oxidation reactions. The most crucial factor of potential barrier height is the work function of the metal electrode, meaning the choice of a suitable metal electrode has a significant effect on the degree of interface oxidation [26]. Moreover, oxygen diffusion through high-*k* oxide during post-device-fabrication processes can also cause formation of an interfacial layer [27]. Diffused oxygen ions leave behind oxygen vacancies that form oxygen deficient layers or intermix with metal electrode elements. Exposure to a high-temperature environment is the most crucial factor for oxygen diffusion, meaning a high-*k* oxide must be thermodynamically stable where it contacts the underlying electrode [28]. From those two reasons above, the adoption of Ru is more advantageous than TiN to suppress a formation of interfacial layer because Ru has larger work function than TiN and is more stable in an oxidizing atmosphere during deposition process and post-device-fabrication processes [29–31].

Because the presence of interfacial layers on the metal electrodes was confirmed by TEM, we characterized the chemical compositions of the interfacial layers using XPS. Fig. 1(c) and (d) present the XPS depth profiles captured after the Ar sputtering (0, 60, 120, 180, and 240 s) of 15-nm-thick ZrO_2 films, where the relative chemical compositions are plotted versus etching time. With an increase in etching time, the concentrations of the ALD ZrO_2 thin film elements gradually decrease, whereas the concentrations of the substrate elements increase. In the case of ALD ZrO_2 on TiN, the atomic contents of Zr-O and Ti-N become very similar after 120 s of etching. This is indicative of element intermixing between the high-*k* layer and bottom electrode. Therefore, the XPS spectra captured at 120 s were further analyzed to perform the detailed comparisons presented in Figs. 2 and 3.

Fig. 2 presents the XPS spectra of the Zr 3d, O 1s, Ti 2p, and N 1s peaks measured from the same sample used in the depth profile analysis presented in Fig. 1(c). Fig. 2(a) presents the Zr 3d XPS spectra of the ZrO_2/TiN sample. In pure ZrO_2, a regular Zr 3d doublet from the Zr (IV) in the oxide arises based on the spin-orbit splitting of Zr $3d_{5/2}$ (182.2

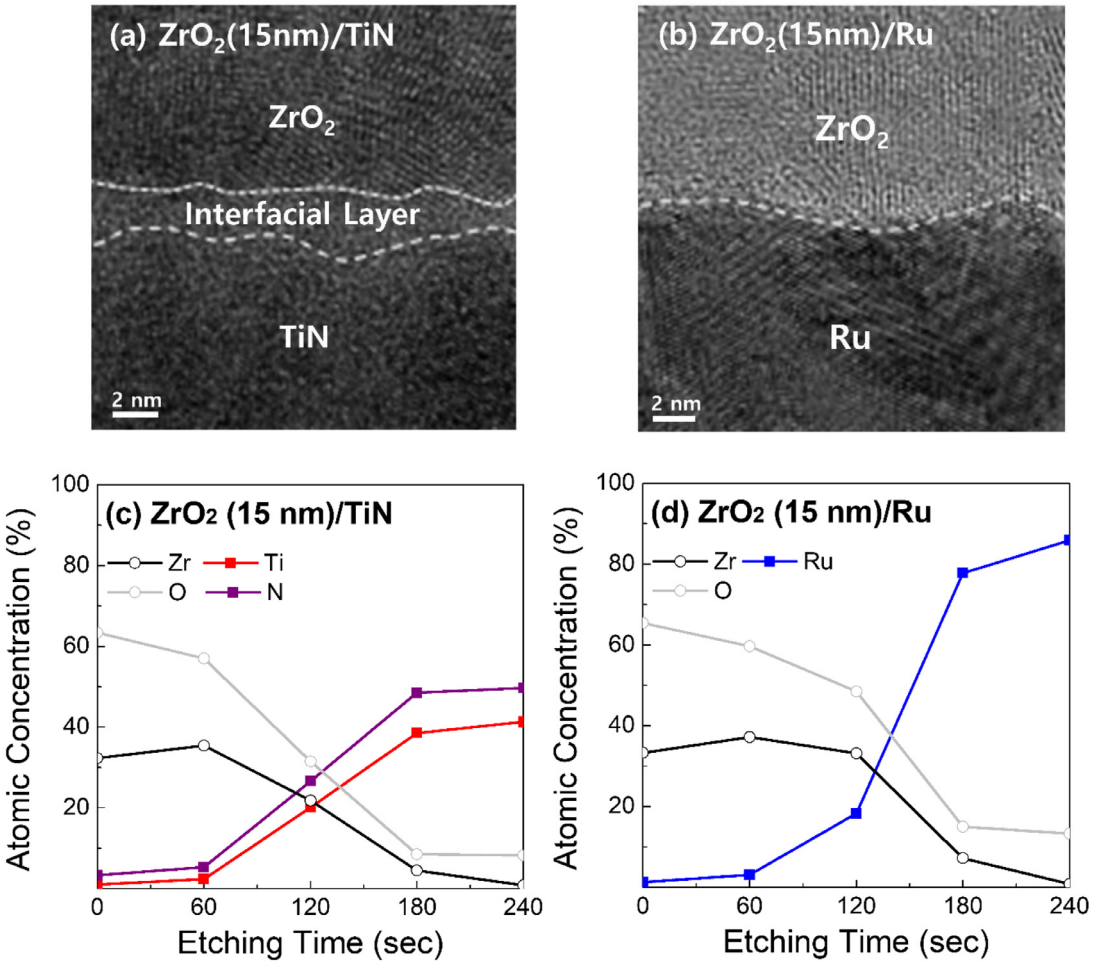

Fig. 1. Cross-sectional TEM images of (a) ZrO_2/TiN and (b) ZrO_2/Ru structures and XPS depth profiles of chemical composition ratio with etching time for (c) ZrO_2/TiN and (d) ZrO_2/Ru structures.

eV) and Zr $3d_{3/2}$ (184.5 eV) [32]. However, in this case, one can see three distinguishable peaks. Based on deconvolution, they were found to originate from the Zr 3d doublet (ZrO_2) mentioned above and the other bonding features of Zr-related sub-oxides, namely oxygen-deficient Zr-oxide (ZrO_x and ZrO_y, $0 < x < y < 2$), Zr sub-oxynitride (ZrO_xN_y), and Zr-Ti sub-oxide materials ($ZrTiO_x$), which are formed through intermixing with the underlying substrate during oxide deposition [33–37]. Their relative atomic compositions were determined to be 8.8%, 21.5%, 31.4%, 16.6%, and 21.7% in order of mention. This indicates that during ZrO_2 ALD, the formation of the interfacial layer observed in Fig. 1(a) is related to various types of sub-oxides generated by intermixing between the growing ZrO_2 and TiN bottom electrode. Fig. 2(b) presents the O 1s XPS spectra of the ZrO_2/TiN samples. Similar to the Zr 3d spectra, they can be deconvoluted to reveal the following chemical bonds: ZrO_2 (14.8%), ZrO_x (20.3%), ZrO_y (21.7%), $ZrTiO_x$ (18.5%), ZrO_xN_y (9.5%), and TiO_xN_y (15.2%) [33,36,38–40]. Similar bonding features can be observed in the XPS spectra of the Ti 2p and N 1s. Fig. 2(c) presents the XPS spectra of the Ti 2p in the ZrO_2/TiN samples. There are three noticeable bonds, namely TiN, $ZrTiO_x$, and TiO_xN_y, whose relative atomic concentrations are 33%, 24.9%, and 26.2%, respectively [36,41,42]. The N 1s spectra in Fig. 2(d) were deconvoluted to reveal TiN, TiO_xN_y, and ZrO_xN_y bonds with relative compositional ratios of 41.7%, 35.8%, and 22.5%, respectively [43–45].

Fig. 3 presents the XPS spectra of the Zr 3d, O 1s, and Ru 3d peaks measured from the sample employed in the depth profile analysis presented in Fig. 1(d). The Zr 3d XPS spectra of the ZrO_2/Ru sample presented in Fig. 3(a) were deconvoluted into three chemical moieties: ZrO_2 (72.6%), ZrO_x (14.1%), and ZrO_y (13.3%) [46,47]. Unlike the Zr 3d spectra in Fig. 2(a), stoichiometric ZrO_2 bonding was largely observed with a relatively small number of sub-oxide moieties based on a lack of intermixing with the underlying Ru substrate. Similarly, as a result of deconvolution of the O 1s XPS spectra presented in Fig. 3(b), we observed that not only was ZrO_2 (80.5%) most of the chemical moieties, but it also possessed a small amount of sub-oxides, namely ZrO_x (8.2%) and ZrO_y (6.5%) [$0 < x < y < 2$] as well as RuO_x (4.8%) [$0 < x < 2$] [37,38,48,49]. In the fitted spectra of the Ru 3d presented in Fig. 3(c), the peak positions of the Ru 3d double agree well with the theoretical spin-orbit splitting of Ru 3d. However, a small number of RuO_x bonds were also found based on the high oxidation potential of O_3 during ZrO_2 deposition. Nevertheless, RuO_x has known to be highly conductive (~20 μΩ cm) with high work function (>5 eV), thereby also being one of the promising candidates for capacitor electrodes in DRAMs [31,50]. The relative atomic compositions of these components were determined to be 95.5% and 4.5%, respectively (Table 2). These results all indicate that the formation of an interfacial layer is significantly influenced by the choice of bottom electrode material. Because Ru has good thermal and chemical stability, using a Ru electrode is beneficial for preventing oxidation, thereby suppressing the formation of sub-oxide moieties with poor electrical qualities [31,51,52].

Finally, the dielectric properties of ALD ZrO_2 films grown on both TiN and Ru bottom electrodes were evaluated through *C–V* and *I–V* measurements of Ru/10-nm-thick ALD ZrO_2/TiN- or Ru-structured MIM capacitors. Fig. 4(a) and (b) present the *C–V* characteristics of the MIM

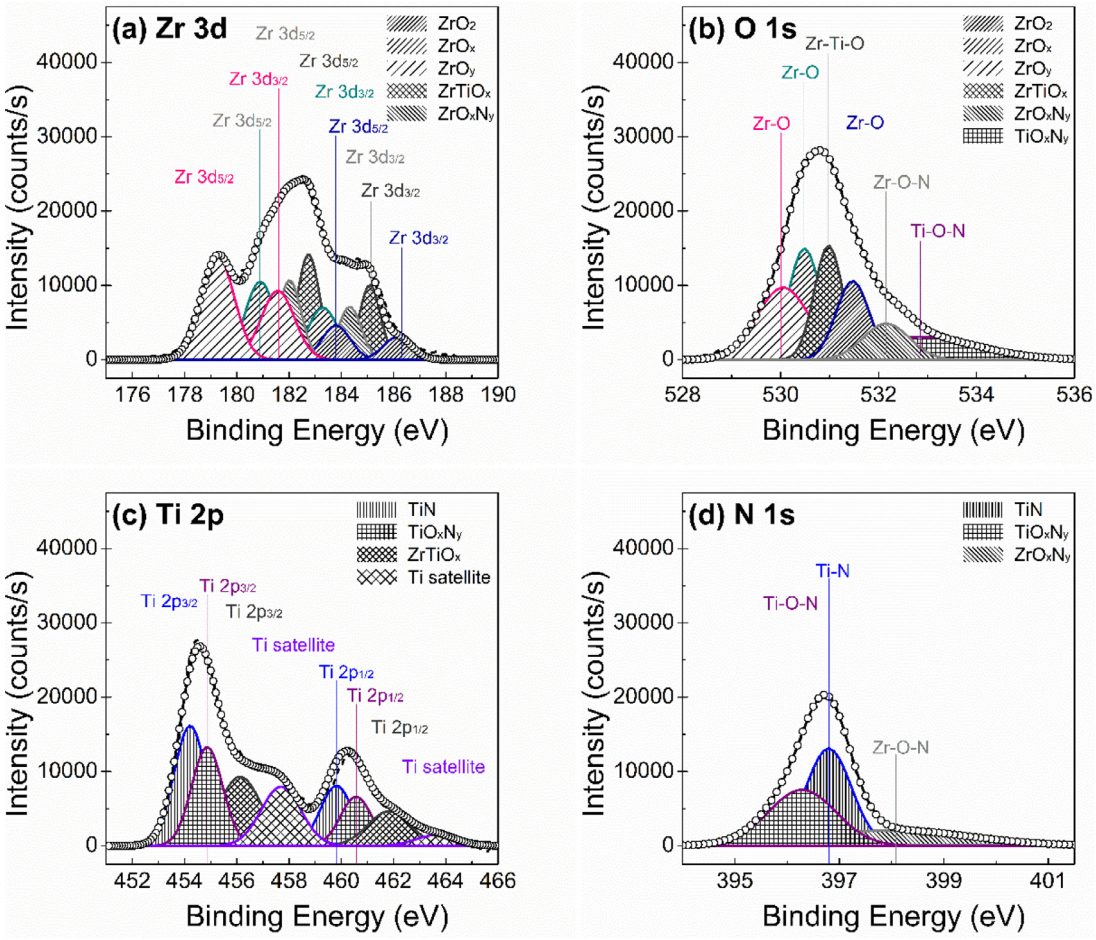

Fig. 2. XPS spectra at 120s etching time of the (a) Zr 3d, (b) O 1s, (c) Ti 2p, and (d) N 1s peaks of the sample that was used in the depth profile analysis presented in Fig. 1(c).

capacitors measured at various frequencies (1 kHz, 10 kHz, 100 kHz, and 1 MHz). As the applied voltage increases from −2 V to 2 V, both capacitance curves level off to nearly constant values. However, the MIM capacitors with TiN bottom electrodes show larger variations (approximately 900 pF) in their capacitance values based on the frequency changes. This phenomenon is referred to as frequency dispersion. In contrast, the MIM capacitors with Ru electrodes exhibited much smaller frequency dispersions (approximately 100 pF). The degree of frequency dispersion can be affected by the existence of interfacial layers [53,54]. Specifically, because interfacial layers are filled with charge traps, the *C–V* characteristics of the dielectric layer are significantly influenced in terms of frequency variation. These phenomena can be explained by the changes in relaxation time with different carrier mobility levels in the charge traps of an insulator [55]. This implies that the greater frequency dispersion in the MIM capacitor with the TiN bottom electrode compared that with the Ru bottom electrode must arise from high charge trap densities in the interfacial layer between the ZrO_2 and TiN. Therefore, to ensure the high stability and accuracy of MIM devices, a Ru bottom electrode is preferable.

Fig. 4(c) and (d) present the normalized *C–V* curves (denoted △C $((C_0\ (V))^{-1})$ of the two different types of MIM capacitors. In the case of the MIM capacitors with TiN electrodes, the normalized *C–V* curves in Fig. 4(c) exhibit asymmetric quadratic shapes with negative secondary quadratic coefficients, whereas the curves of the Ru electrodes in Fig. 4(d) exhibit relatively symmetric secondary quadratic curves with positive secondary quadratic coefficients. Not only do normalized *C–V* characteristics indicate the degree of changes in capacitance relative to changes in voltage, which is referred to as voltage linearity, but they also indicate the stability of MIM devices with different metal electrodes. The MIM device with ideal ZrO_2 has positive secondary quadratic coefficients [56]. whereas the current-normalized *C–V* curves for the TiN electrode have negative secondary quadratic coefficients. This can be explained by the electrode polarization mechanism. When voltage is applied to a metal electrode, mobile carriers generated by oxygen vacancies create an accumulation layer, which leads to double-layer capacitance that can trigger changes in capacitance based on voltage variation [16]. Therefore, the second-order quadratic coefficients of the MIM device can change when two or more materials are deposited between the MIM device electrodes. This phenomenon is called a compensation effect. In previous studies on the interfacial layers between ALD ZrO_2 and TiN electrodes, it was found that $ZrTiO_x$, which has negative secondary quadratic coefficients, is one of the main components of the interfacial layers. Based on the presence of $ZrTiO_x$ beneath the ZrO_2 layer, which has positive quadratic coefficients, a negative second-order quadratic coefficient can be induced and normalized to *C–V* curves with the negative second-order quadratic function [57]. In contrast, the MIM capacitor with the Ru electrode formed a positive second-order quadratic function based on the absence of interfacial components with negative second-order quadratic coefficients. Additionally, the stability of MIM capacitors can be negatively affected by the charge traps generated by oxygen vacancies or oxygen interstitials. The asymmetric shape of the resulting *C–V* curves can be attributed to electron injection from the electrode into the dielectric layer, which results in capturing in oxide charge traps [58]. Charge trap density must be suppressed during high-*k* deposition to obtain good voltage linearity. Therefore, it can be concluded that the interfacial

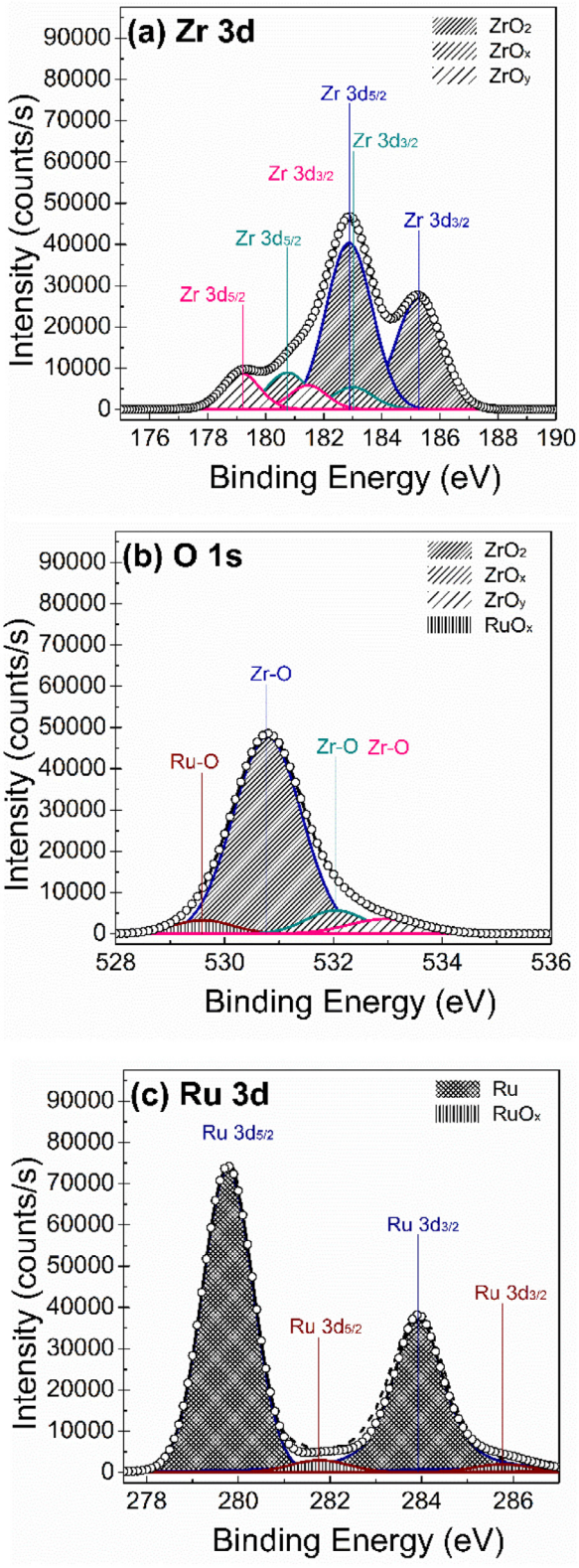

Fig. 3. XPS spectra at 120s etching time of the (a) Zr 3d, (b) O 1s, and (c) Ru 3d peaks of the same sample that was used in the depth profile analysis presented in Fig. 1(d).

layer charge traps formed between high-*k* oxides and underlying metals result in the degradation of the electrical properties of MIM capacitors. Therefore, the formation of interfacial layers must be suppressed during high-*k* deposition to obtain *C–V* characteristics with good voltage linearity and symmetry.

Table 2
Relative surface composition data obtained by XPS analysis of the (a) ZrO_2/TiN and (b) ZrO_2/Ru films after 120s etching time.

Sample	Relative atomic composition (%) (a) ZrO_2/TiN after 120-s etching				(b) ZrO_2/Ru after 120-s etching		
Element	Zr	O	Ti	N	Zr	O	Ru
%	21.8	31.5	20.1	26.6	33.2	48.5	18.3

Fig. 5(a) and (b) present the leakage currents of MIM capacitors with the two different bottom electrodes. One can see that using the TiN electrode leads to leakage currents approximately five times greater than those generated by the Ru electrode. Additionally, injected electrons in the charge traps of interfacial layers can trigger trap-assisted Poole–Frenkel conduction and Schottky emission, resulting in increased leakage current density [59,60]. Based on the above *C–V* and *I–V* results for both MIM capacitors, we can conclude that controlling the formation of interfacial layers plays a critical role in achieving improved electrical properties. Therefore, the results above that indicate improved electrical properties when using Ru electrodes can provide helpful insights into the fabrication of high-quality MIM capacitors.

4. Conclusion

In conclusion, we confirmed different interfacial layer formation behaviors during ZrO_2 ALD processes on TiN and Ru bottom electrodes through TEM observations. In the case of TiN, the thickness of the interfacial layer was measured to be approximately 3 nm. In contrast, negligible interfacial layer formation was observed on the Ru. Based on XPS analysis, the interfacial layer between ALD ZrO_2 and TiN was found to contain various forms of sub-oxide moieties, such as ZrO_x, $ZrTiO_x$, ZrO_xN_y, and TiO_xN_y, whereas that between ALD ZrO_2 and Ru was largely composed of stoichiometric ZrO_2 and small amounts of ZrO_x and RuO_x. Through comparative investigation of the electrical properties of MIM capacitors using both types of bottom electrodes, greater frequency dispersions and asymmetric quadratic curves with negative secondary quadratic coefficients in the *C–V* curves, as well as higher leakage currents in the *I–V* curves, were identified for the MIM capacitors with TiN bottom electrodes. This result is attributed to high charge trap densities in the thick interfacial layer between ZrO_2 and TiN. Therefore, the suppression of interfacial layer formation during high-*k* deposition is crucial for achieving improved electrical properties (Table 3).

CRediT authorship contribution statement

Jae Hwan Lee: Conceptualization, Methodology, Validation, Formal analysis, Investigation, Data curation, Writing - original draft, Writing - review & editing, Visualization. **Bo-Eun Park:** Formal analysis, Investigation, Writing - original draft. **David Thompson:** Resources. **Myeonggi Choe:** Investigation, Visualization. **Zonghoon Lee:** Investigation, Resources. **Il-Kwon Oh:** Conceptualization, Writing - review & editing, Supervision. **Woo-Hee Kim:** Conceptualization, Resources, Writing - review & editing, Supervision, Project administration, Funding acquisition. **Hyungjun Kim:** Conceptualization, Resources, Writing - review & editing, Supervision, Project administration, Funding acquisition.

Declaration of Competing Interest

The authors declare that they have no known competing financial interests or personal relationships that could have appeared to influence the work reported in this paper.

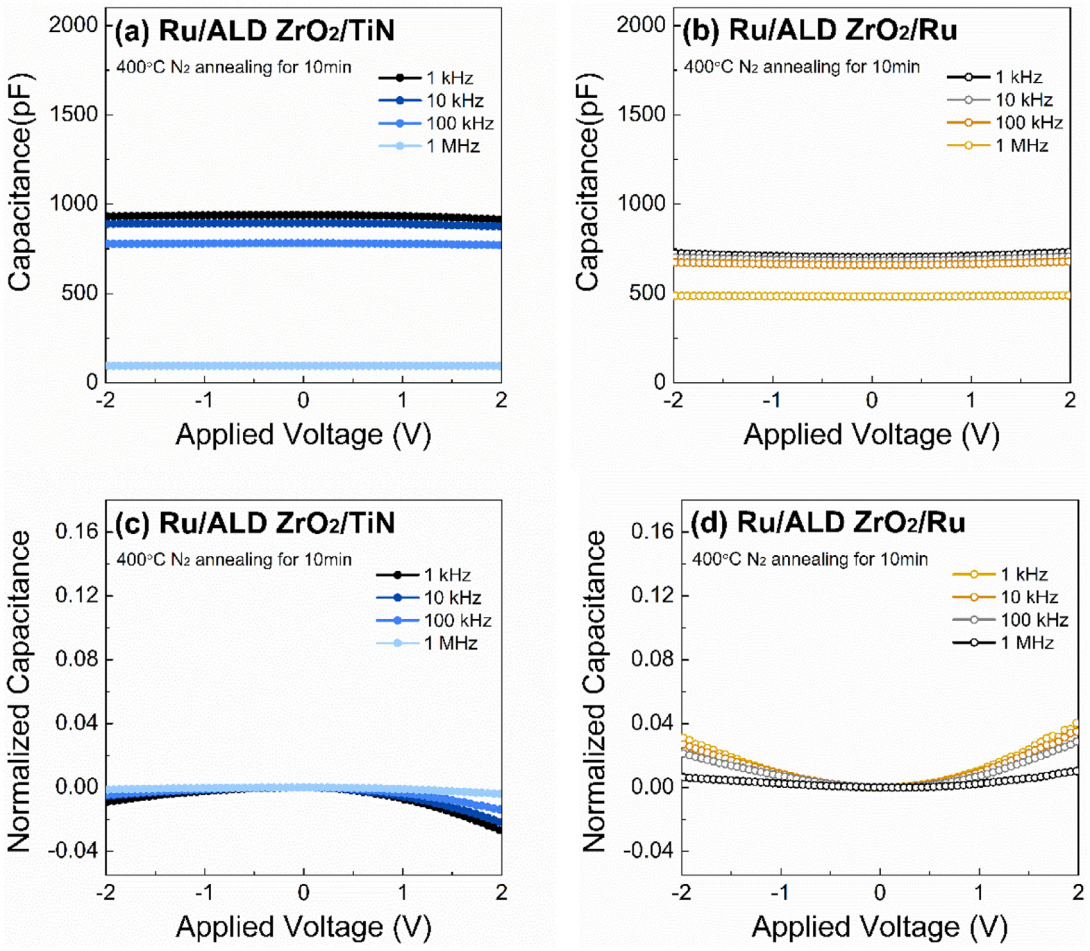

Fig. 4. (a,b) *C–V* curves and (c,d) Normalized *C–V* curves of MIM capacitors with 10-nm-thick ALD ZrO_2 layers on TiN and Ru bottom electrodes.

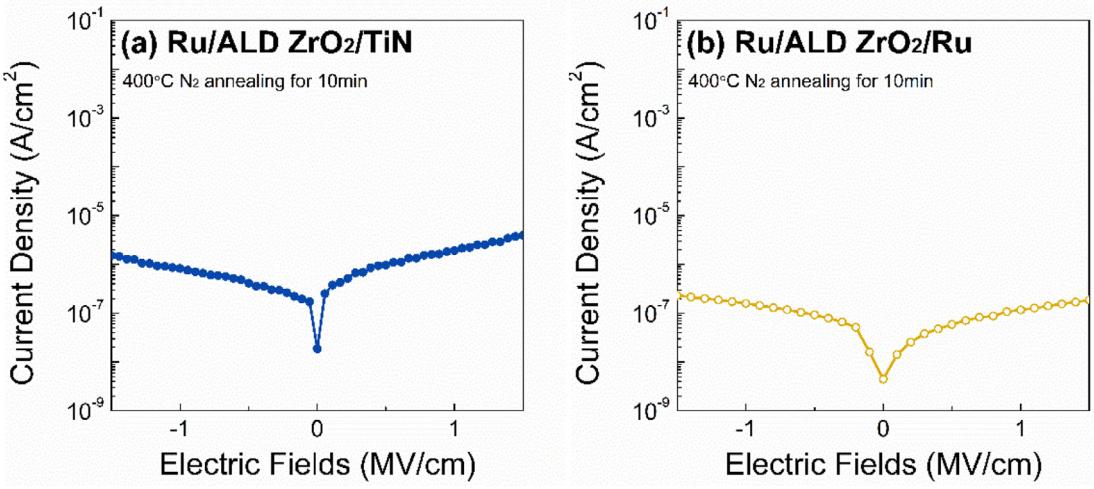

Fig. 5. *I–V* curves of MIM capacitors with 10-nm-thick ALD ZrO_2 layers on (a) TiN and (b) Ru bottom electrodes

Table 3
A comparison of leakage currents in ZrO_2 films deposited on different metal bottom substrates (a) TiN and (b) Ru.

MIM Structure	Leakage Current (A cm^{-2} at −1 V)
$Ru/ZrO_2/TiN$	8.24×10^{-7}
$Ru/ZrO_2/Ru$	1.58×10^{-7}

Acknowledgments

This work was supported by the National Research Foundation of Korea (NRF) grant funded by the Korea government (MSIT) (Nos. NRF-2018R1A2B6005289 and NRF-2017R1C1B5076821). This research was supported by the MOTIE (Ministry of Trade, Industry & Energy, No. 20006504 and No. 20007000) and KSRC (Korea Semiconductor Research Consortium) support program for the development of the

future semiconductor device. Following are results of a study on the "Leaders in Industry-university Cooperation +" Project, supported by the Ministry of Education and National Research Foundation of Korea. This work was also supported by Air Liquide as a precursor supplier.

References

[1] I.S. Devised, I. For, T. Assessment, I.S. Without, R. To, C. Considerations, P. To, I. Products, O.R. Equipment, I Nternational T Echnology R Oadmap for, 2015.

[2] C. Wenger, M. Lukosius, G. Weidner, H.J. Müssig, S. Pasko, C. Lohe, The role of the HfO_2-TiN interface in capacitance-voltage nonlinearity of metal-insulator-metal capacitors, Thin Solid Films 517 (2009) 6334–6336, https://doi.org/10.1016/j.tsf.2009.02.074.

[3] N. Menou, M. Popovici, K. Opsomer, B. Kaczer, M.A. Pawlak, C. Adelmann, A. Franquet, P. Favia, H. Bender, C. Detavernier, S. Van Elshocht, D.J. Wouters, S. Biesemans, J.A. Kittl, Seed layer and multistack approaches to reduce leakage in $SrTiO_3$-based metal-insulator-metal capacitors using TiN bottom electrode, Jpn. J. Appl. Phys. 49 (2010), https://doi.org/10.1143/JJAP.49.04DD01.

[4] M. Lukosius, C.B. Kaynak, C. Wenger, G. Ruhl, S. Rushworth, P. Baumann, Atomic Vapor Depositions of Ti-Ta-O thin films for Metal-Insulator-Metal applications, Thin Solid Films 519 (2011) 3831–3834, https://doi.org/10.1016/j.tsf.2011.01.239.

[5] W. Weinreich, R. Reiche, M. Lemberger, G. Jegert, J. Müller, L. Wilde, S. Teichert, J. Heitmann, E. Erben, L. Oberbeck, U. Schröder, A.J. Bauer, H. Ryssel, Impact of interface variations on *J–V* and *C–V* polarity asymmetry of MIM capacitors with amorphous and crystalline $Zr_{(1-x)}Al_xO_2$ films, Microelectron. Eng. 86 (2009) 1826–1829, https://doi.org/10.1016/j.mee.2009.03.070.

[6] M.K. Kim, W.H. Kim, T. Lee, H. Kim, Growth characteristics and electrical properties of Ta_2O_5 grown by thermal and O_3-based atomic layer deposition on TiN substrates for metal-insulator-metal capacitor applications, Thin Solid Films 542 (2013) 71–75, https://doi.org/10.1016/j.tsf.2013.06.050.

[7] N.K. Park, D.K. Kang, B.H. Kim, S.J. Jo, J.S. Ha, Electrical properties of La_2O_3 thin films grown on TiN/Si substrates via atomic layer deposition, Appl. Surf. Sci. 252 (2006) 8506–8509, https://doi.org/10.1016/j.apsusc.2005.11.064.

[8] T. Boscke, S. Kudelka, A. Sanger, J. Muller, W. Krautschneider, Investigation of the high temperature stability of TiN-Al_2O_3-TiN capacitors for sub 50nm deep trench DRAM, 2006 Eur. Solid-State Device Res. Conf. 2006, pp. 391–394, , https://doi.org/10.1109/ESSDER.2006.307720.

[9] D. Misra, J. Kasinath, A.N. Chandorkar, Voltage and current stress induced variations in TiN/$HfSi_xO_y$/TiN MIM capacitors, Microelectron. Reliab. 53 (2013) 270–273, https://doi.org/10.1016/j.microrel.2012.08.020.

[10] T.S. Jeon, J.M. White, D.L. Kwong, Thermal stability of ultrathin ZrO_2 films prepared by chemical vapor deposition on Si(100), Appl. Phys. Lett. 78 (2001) 368, https://doi.org/10.1063/1.1339994.

[11] W.J. Qi, R. Nieh, B.H. Lee, L. Kang, Y. Jeon, J.C. Lee, Electrical and reliability characteristics of ZrO_2 deposited directly on Si for gate dielectric application, Appl. Phys. Lett. 77 (2000) 3269–3271, https://doi.org/10.1063/1.1326482.

[12] Q. Zhang, The effects of annealing on the electrical performance of MIM capacitors with ZrO_2 dielectric, Integr. Ferroelectr. 199 (2019) 112–117, https://doi.org/10.1080/10584587.2019.1592604.

[13] B.E. Park, I.K. Oh, C. Mahata, C.W. Lee, D. Thompson, H.B.R. Lee, W.J. Maeng, H. Kim, Atomic layer deposition of Y-stabilized ZrO_2 for advanced DRAM capacitors, J. Alloys Compd 722 (2017) 307–312, https://doi.org/10.1016/j.jallcom.2017.06.036.

[14] M. Pešić, S. Knebel, K. Cho, C. Jung, J. Chang, H. Lim, N. Kolomiiets, V.V. Afanas'ev, T. Mikolajick, U. Schroeder, Conduction barrier offset engineering for DRAM capacitor scaling, Solid. State. Electron. 115 (2016) 133–139, https://doi.org/10.1016/j.sse.2015.08.012.

[15] T.H. Perng, C.H. Chien, C.W. Chen, P. Lehnen, C.Y. Chang, High-density MIM capacitors with HfO_2 dielectrics, Thin Solid Films 469–470 (2004) 345–349, https://doi.org/10.1016/j.tsf.2004.08.148.

[16] C. Jorel, C. Vallée, E. Gourvest, B. Pelissier, M. Kahn, M. Bonvalot, P. Gonon, Physicochemical and electrical characterizations of atomic layer deposition grown HfO_2 on TiN and Pt for metal-insulator-metal application, J. Vac. Sci. Technol. B Microelectron. Nanom. Struct. 27 (2009) 378, https://doi.org/10.1116/1.3021036.

[17] C.H. Cheng, H.C. Pan, C.C. Huang, C.P. Chou, C.N. Hsiao, J. Hu, M. Hwang, T. Arikado, S.P. McAlister, A. Chin, Improvement of the performance of TiHfO MIM capacitors by using a dual plasma treatment of the lower electrode, IEEE Electron Device Lett. 29 (2008) 1105–1107, https://doi.org/10.1109/LED.2008.2000945.

[18] K. Kim, I.K. Oh, H. Kim, Z. Lee, Atomic-scale characterization of plasma-induced damage in plasma-enhanced atomic layer deposition, Appl. Surf. Sci. 425 (2017) 781–787, https://doi.org/10.1016/j.apsusc.2017.06.241.

[19] C. Vallée, P. Gonon, C. Jorel, F. El Kamel, M. Mougenot, V. Jousseaume, High j for MIM and RRAM applications : impact of the metallic electrode and oxygen vacancies, Microelectron. Eng. 86 (2009) 1774–1776, https://doi.org/10.1016/j.mee.2009.03.001.

[20] J.H. Ahn, S.H. Kwon, Sub-0.5 nm equivalent oxide thickness scaling for Si-doped $Zr_{1-x}Hf_xO_2$ thin film without using noble metal electrode, ACS Appl. Mater. Interfaces. 7 (2015) 15587–15592, https://doi.org/10.1021/acsami.5b04303.

[21] S.J. Park, W.H. Kim, H.B.R. Lee, W.J. Maeng, H. Kim, Thermal and plasma enhanced atomic layer deposition ruthenium and electrical characterization as a metal electrode, Microelectron. Eng. 85 (2008) 39–44, https://doi.org/10.1016/j.mee.2007.01.239.

[22] W.H. Kim, S.J. Park, J.Y. Son, H. Kim, Ru nanostructure fabrication using an anodic aluminum oxide nanotemplate and highly conformal Ru atomic layer deposition, Nanotechnology 19 (2008), https://doi.org/10.1088/0957-4484/19/04/045302.

[23] G.J. Choi, S.K. Kim, S.Y. Lee, W.Y. Park, M. Seo, B.J. Choi, C.S. Hwang, Atomic layer deposition of TiO_2 films on Ru buffered TiN electrode for capacitor applications, J. Electrochem. Soc. 156 (2009) 71–77, https://doi.org/10.1149/1.3125713.

[24] A Tsuzumitani, Y Okuno, J Shibata, T Shimizu, K Yamamoto, Y Mori, Extendibility of Ta_2O_5 metal-insulator-metal capacitor using Ru electrode, Jpn. J. Appl. Phys. 39 (2000) 2073–2077, https://doi.org/10.1143/JJAP.39.2073.

[25] M. Ritala, K. Kukli, A. Rahtu, P.I. Räisänen, M. Leskelä, T. Sajavaara, J. Keinonen, Atomic layer deposition of oxide thin films with metal alkoxides as oxygen sources, Science (80-.). 288 (2000) 319–321, https://doi.org/10.1126/science.288.5464.319.

[26] W.G. Kim, S.W. Rhee, Effect of the top electrode material on the resistive switching of TiO_2 thin film, Microelectron. Eng. 87 (2010) 98–103, https://doi.org/10.1016/j.mee.2009.05.023.

[27] A. Ogawa, K. Iwamoto, H. Ota, Y. Morita, M. Ikeda, T. Nabatame, A. Toriumi, 0.6nm-EOT high-*k* gate stacks with $HfSiO_x$ interfacial layer grown by solid-phase reaction between HfO_2 and Si substrate, Microelectron. Eng. 84 (2007) 1861–1864, https://doi.org/10.1016/j.mee.2007.04.005.

[28] I.K. Oh, G. Yoo, C.M. Yoon, T.H. Kim, G.Y. Yeom, K. Kim, Z. Lee, H. Jung, C.W. Lee, H. Kim, H.B.R. Lee, Very high frequency plasma reactant for atomic layer deposition, Appl. Surf. Sci. 387 (2016) 109–117, https://doi.org/10.1016/j.apsusc.2016.06.048.

[29] J.H. Kim, S.G. Yoon, S.J. Yeom, H.K. Woo, D.S. Kil, J.S. Roh, H.C. Sohn, Electrical properties in high-*k* HfO_2 capacitors with an equivalent oxide thickness of 9Å on Ru metal electrode, Electrochem. Solid-State Lett. 8 (2005) 19–21, https://doi.org/10.1149/1.1895285.

[30] G. Giusi, M. Aoulaiche, J. Swerts, M. Popovici, A. Redolfi, E. Simoen, M. Jurczak, Impact of electrode composition and processing on the low-frequency noise in $SrTiO_3$ MIM capacitors, IEEE Electron Device Lett. 35 (2014) 942–944, https://doi.org/10.1109/LED.2014.2335771.

[31] T.E. Hong, S.H. Choi, S. Yeo, J.Y. Park, S.H. Kim, T. Cheon, H. Kim, M.K. Kim, H. Kim, Atomic layer deposition of Ru thin films using a Ru(0) metallorganic precursor and O_2, ECS J. Solid State Sci. Technol. 2 (2013), https://doi.org/10.1149/2.001303jss.

[32] J. Liu, M. Liao, M. Imura, A. Tanaka, H. Iwai, Y. Koide, Low on-resistance diamond field effect transistor with high-*k* ZrO_2 as dielectric, Sci. Rep. 4 (2014) 2–6, https://doi.org/10.1038/srep06395.

[33] A. Roustila, J. Chêne, C. Séverac, XPS study of hydrogen and oxygen interactions on the surface of zirconium, J. Alloys Compd. 356–357 (2003) 330–335.

[34] I. Bespalov, M. Datler, S. Buhr, W. Drachsel, G. Rupprechter, Y. Suchorski, Initial stages of oxide formation on the Zr surface at low oxygen pressure: An in situ FIM and XPS study, Ultramicroscopy 159 (2015) 147–151, https://doi.org/10.1016/j.ultramic.2015.02.016.

[35] D. Roman, J. Bernardi, C.L.G.D. Amorim, F.S. De Souza, A. Spinelli, C. Giacomelli, C.A. Figueroa, I.J.R. Baumvol, R.L.O. Basso, Effect of deposition temperature on microstructure and corrosion resistance of ZrN thin films deposited by DC reactive magnetron sputtering, Mater. Chem. Phys. 130 (2011) 147–153, https://doi.org/10.1016/j.matchemphys.2011.06.013.

[36] H. Ikawa, T. Yamada, K. Kojima, S. Matsumoto, X-ray Photoelectron Spectroscopy Study of high- and low-temperature forms of zirconium titanate, J. Am. Ceram. Soc. 74 (1991) 1459–1462, https://doi.org/10.1111/j.1151-2916.1991.tb04131.x.

[37] M. Chun, M.J. Moon, J. Park, Y.C. Kang, Physical and chemical investigation of substrate temperature dependence of zirconium oxide films on Si(100), Bull. Korean Chem. Soc. 30 (2009) 2729–2734, https://doi.org/10.5012/bkcs.2009.30.11.2729.

[38] G.X. Liu, A. Liu, Y. Meng, F.K. Shan, B.C. Shin, W.J. Lee, C.R. Cho, Annealing dependence of solution-processed ultra-thin ZrO_x films for gate dielectric applications, J. Nanosci. Nanotechnol. 15 (2015) 2185–2191, https://doi.org/10.1166/jnn.2015.10228.

[39] G.I. Cubillos, M. Bethencourt, J.J. Olaya, Corrosion resistance of zirconium oxynitride coatings deposited via DC unbalanced magnetron sputtering and spray pyrolysis-nitriding, Appl. Surf. Sci. 327 (2015) 288–295, https://doi.org/10.1016/j.apsusc.2014.11.168.

[40] A. Vesel, M. Mozetic, J. Kovac, A. Zalar, XPS study of the deposited Ti layer in a magnetron-type sputter ion pump, Appl. Surf. Sci. 253 (2006) 2941–2946, https://doi.org/10.1016/j.apsusc.2006.06.033.

[41] Jong-Chang Woo, Chang-Auck Choi, Young-Hee Joo, Han-Soo Kim, C.-I. Kim, The dry etching of TiN thin films using inductively coupled CF_4/Ar plasma, Trans. Electr. Electron. Mater. 14 (2013) 67–70, https://doi.org/10.4313/teem.2003.4.3.001.

[42] V. Stranak, M. Quaas, R. Bogdanowicz, H. Steffen, H. Wulff, Z. Hubicka, M. Tichy, R. Hippler, Effect of nitrogen doping on TiO_xN_y thin film formation at reactive high-power pulsed magnetron sputtering, J. Phys. D. Appl. Phys. 43 (2010), https://doi.org/10.1088/0022-3727/43/28/285203.

[43] G.M. Ingo, S. Kaciulis, A. Mezzi, T. Valente, F. Casadei, G. Gusmano, Characterization of composite titanium nitride coatings prepared by reactive plasma spraying, Electrochim. Acta. 50 (2005) 4531–4537, https://doi.org/10.1016/j.electacta.2004.10.089.

[44] B. Avasarala, P. Haldar, Electrochemical oxidation behavior of titanium nitride based electrocatalysts under PEM fuel cell conditions, Electrochim. Acta. 55 (2010) 9024–9034, https://doi.org/10.1016/j.electacta.2010.08.035.

[45] G.I. Cubillos, M. Bethencourt, J.J. Olaya, J.E. Alfonso, J.F. Marco, The influence of deposition temperature on microstructure and corrosion resistance of ZrO_xN_y /ZrO_2 coatings deposited using RF sputtering, Appl. Surf. Sci. 309 (2014) 181–187, https://doi.org/10.1016/j.apsusc.2014.04.215.

[46] S. Sinha, S. Badrinarayanant, A.P.B. Sinha, Interaction of oxygen with $Zr_{76}Fe_{24}$ metglass: an X-ray photoelectron spectroscopy study, J. Less Common Met. 125

(1986) 85–95.
[47] Y.M. Wang, Y.S. Li, P.C. Wong, K.A.R. Mitchell, XPS studies of the stability and reactivity of thin films of oxidized zirconium, Appl. Surf. Sci. 72 (1993) 237–244, https://doi.org/10.1016/0169-4332(93)90192-E.
[48] W. Cao, W. Luo, H. Ge, Y. Su, A. Wang, T. Zhang, UiO-66 derived Ru/ZrO_2@C as a highly stable catalyst for hydrogenation of levulinic acid to γ-valerolactone, Green Chem. 19 (2017) 2201–2211, https://doi.org/10.1039/c7gc00512a.
[49] M. Zhang, W. Chen, S.J. Ding, Z.Y. Liu, Y. Huang, Z.W. Liao, D.W. Zhang, Physical and electrical characterization of atomic-layer-deposited Ru nanocrystals embedded into Al_2O_3 for memory applications, J. Phys. D. Appl. Phys. 41 (2008), https://doi.org/10.1088/0022-3727/41/3/032007.
[50] K. Hušeková, E. Dobročka, A. Rosová, J. Šoltýs, A. Šatka, F. Fillot, K. Fröhlich, Growth of RuO_2 thin films by liquid injection atomic layer deposition, Thin Solid Films 518 (2010) 4701–4704, https://doi.org/10.1016/j.tsf.2009.12.063.
[51] A. Das, S. Maikap, C.H. Lin, P.J. Tzeng, T.C. Tien, T.Y. Wangd, L.B. Chang, J.R. Yang, M.J. Tsai, Ruthenium oxide metal nanocrystal capacitors with high-K dielectric tunneling barriers for nanoscale nonvolatile memory device applications, Microelectron. Eng. 87 (2010) 1821–1827, https://doi.org/10.1016/j.mee.2009.10.028.
[52] B.S. Lee, Y.C. Choi, Preparation of Pt/Ru bilayers and their application to the capacitor of memory devices, Japanese J. Appl. Physics, Part 1 Regul. Pap. Short Notes Rev. Pap. 39 (2000) 222–226, https://doi.org/10.1143/JJAP.39.222.
[53] C. Zhao, C.Z. Zhao, M. Werner, S. Taylor, P. Chalker, P. King, Grain size dependence of dielectric relaxation in cerium oxide as high-*k* layer, Nanoscale Res. Lett. 8 (2013) 1–10, https://doi.org/10.1186/1556-276X-8-172.
[54] M.K. Bera, C. Mahata, A.K. Chakraborty, S.K. Nandi, J.N. Tiwari, J.Y. Hung, C.K. Maiti, TiO_2/GeO_xN_y stacked gate dielectrics for Ge-MOSFETs, Semicond. Sci. Technol. 22 (2007) 1352–1361, https://doi.org/10.1088/0268-1242/22/12/020.
[55] J. De Chen, J.J. Yang, R. Wise, P. Steinmann, M. Bin Yu, C. Zhu, Y.C. Yeo, Physical and electrical characterization of metal-insulator-metal capacitors with Sm_2O_3 and Sm_2O_3/SiO_2 laminated dielectrics for analog circuit applications, IEEE Trans. Electron Devices. 56 (2009) 2683–2691, https://doi.org/10.1109/TED.2009.2030539.
[56] C. Jorel, C. Valĺe, P. Gonon, E. Gourvest, C. Dubarry, E. Defay, High performance metal-insulator-metal capacitor using a $SrTiO_3$/ ZrO_2 bilayer, Appl. Phys. Lett. 94 (2009) 6–9, https://doi.org/10.1063/1.3158951.
[57] L.L. Chen, Y.H. Wu, Y.B. Lin, C.C. Lin, M.L. Wu, $ZrLaO_x/ZrTiO_x/ZrLaO_x$ laminate as insulator for mim capacitors with high capacitance density and low quadratic voltage coefficient using canceling effect, IEEE Electron Device Lett. 33 (2012) 1447–1449, https://doi.org/10.1109/LED.2012.2209396.
[58] C. Park, S.D. Park, D.C. Gilmer, H.K. Park, C.Y. Kang, K.Y. Lim, C. Burham, J. Barnett, P.D. Kirsch, H.H. Tseng, R. Jammy, G.Y. Yeom, Bulk and Interface effects on voltage linearity of ZrO_2 - SiO_2 multilayered metal-insulator-metal capacitors for analog mixed-signal applications, Appl. Phys. Lett. 95 (2009), https://doi.org/10.1063/1.3182856.
[59] K.C. Chiang, C.C. Huang, G.L. Chen, W.J. Chen, H.L. Kao, Y.H. Wu, A. Chin, S.P. McAlister, High-performance $SrTiO_3$ MIM capacitors for analog applications, IEEE Trans. Electron Devices. 53 (2006) 2312–2318, https://doi.org/10.1109/TED.2006.881013.
[60] F.C. Chiu, A review on conduction mechanisms in dielectric films, Adv. Mater. Sci. Eng. 2014 (2014), https://doi.org/10.1155/2014/578168.